Microwave-assisted synthesis of anhydrous lanthanide-based coordination polymers built upon benzene-1,2,4,5-tetracarboxylic acid

Thibault Amiaud, Nicolas Stephant, Rémi Dessapt, Hélène Serier-Brault

Microwave-assisted synthesis of anhydrous lanthanide-based coordination polymers built upon benzene-1,2,4,5-tetracarboxylic acid

Thibault Amiaud, Nicolas Stephant, Rémi Dessapt, and Hélène Serier-Brault*

Université de Nantes, CNRS, Institut des Matériaux Jean Rouxel, IMN 44000 Nantes, France
E-mail: helene.brault@cnrs-imn.fr

Abstract: A series of trivalent lanthanide and group 3 metal coordination polymers with pyromellitic acid $[M(Hbtec)]_n$ (M = Eu, Dy, Sm, Nd, Ce, Er, Y) has been synthesized and structurally characterized. Contrary to most of coordination polymers, the reported compounds do not present any crystallized solvent molecules, and consequently they are thermally stable until 400-500°C. Moreover, they also exhibit good stability in water on a wide pH range. Compounds were synthesized by hydrothermal route with conventional heating but also with microwave-assisted heating, allowing to noticeably reduce the synthesis time to 1h max. Efforts have been done to obtain nanoparticles with this strategy. Finally, the luminescence properties of the lanthanide counterparts emitting in the visible range (Dy, Sm, Eu) were thoroughly investigated, and the Eu compound exhibit good quantum yield.

Introduction

Lanthanide coordination polymers is a fascinating class of materials which is widely investigated due to their potential applications in gas storage [1–6], catalysis [7], magnetism [8–12] or luminescence [13–17]. Most of them are built with benzoic multicarboxylate ligands which are versatile building blocks to obtain various coordination polymers due to their variety of bridging abilities [2,18–20]. Among the various suitable multicarboxylate ligands, the ligand 1,2,4,5-benzenetetracarboxylic acid (also called pyromellitic acid) exhibits numerous features which make it very attractive to design coordination polymers. First, this ligand offers different coordination modes because it can be partially or totally deprotonated. Then, the carboxylate groups do not lie in the phenyl plane which favor a huge structure diversity and finally its π system renders its suitable to sensitize Ln^{3+} excited levels according an efficient antenna effect [21].

Numerous lanthanide-bearing coordination polymers involving this linker have been already reported by using hydrothermal routes [22–27]. However, most of them contain coordinated or non-coordinated water molecules which can limit their thermal stability with a crystal structure collapsing after dehydration. Furthermore, lanthanide coordination polymers are significantly investigated for luminescence, and the presence of water molecules may promote non radiative deactivation process, and consequently luminescence quenching. Here, we report a family of seven coordination polymers based on $Hbetc^{3-}$, namely $[M(Hbtec)]_n$ (M = Eu, Sm, Nd, Er, Ce, Y, Dy). Their crystal structure has been solved by single-crystal X-ray diffraction and they are isostructural to Tb and Gd counterparts[28,29], already reported in the literature as luminescent market for gunshot, and for magnetic properties, respectively. Herein, we evidenced that almost the whole lanthanide series can be obtained, from Ce to Er, some of lanthanide coordination polymers being missing. Moreover, most of compounds have been easily obtained by microwave-assisted hydrothermal route with a very short synthesis duration and good chemical yields. Furthermore, several attempts have been performed to reduce the grain size of microcrystalline powder of the Eu counterpart by tuning experimental parameters (temperature, synthesis duration, metal precursor nature, microwave power, use of steric agent), the grain size reduction being a requirement to enhance sensitivity for

chemical sensing. Thermal and chemical stability have been also thoroughly investigated by powder XRD. Finally, the luminescence properties (emission, lifetimes and quantum yields) of the Eu, Sm and Dy counterparts have been studied.

Materials and methods

Synthesis of single-crystal compounds. All the reagents of analytical grade were obtained from commercial sources and used without further purification.

All single-crystals compounds were obtained according to a similar procedure than reported in the literature.[28,29] A mixture of $Ln(NO_3)_3 \cdot xH_2O$ (0.75 mmol), 1,2,4,5-benzenetetracarboxylic acid (381.2 mg, 1.5 mmol) and H_2O (15 mL) was sealed in a stainless-steel reactor with Teflon liner. Then, the mixture was heated at 180° C for 3 days under autogenous pressure and slowly cooled down to room temperature. Small crystals were finally recovered by filtration and washed successively with H_2O and EtOH.

[Eu(HBtec)]$_n$ (*Eu-conv*). Yield: 0.120 g (40 %). Anal. Calcd for $EuC_{10}O_8H_3$ (%): C, 29.8; H, 0.75. Found: C, 29.7; H, 0.65. IR (KBr pellet, cm^{-1}): 1676 (vs), 1614 (m), 1572 (vs), 1531 (vs), 1493 (vs), 1464 (m), 1393 (vs), 1342(vs), 1271 (s), 1256 (vs), 1182 (m), 1140 (m), 1003 (m), 930 (m), 905 (m), 878 (m), 854 (s), 808 (s), 793 (s), 766 (m), 731 (s), 712 (s), 621 (s), 546 (s), 496 (s), 438 (s).

[Dy(HBtec)]$_n$ (*Dy-conv*). Yield: 0.200 g (64 **%**). Anal. Calcd for $DyC_{10}O_8H_2$ (%): C, 29.1; H, 0.49. Found: C, 28.6; H, 0.33. IR (KBr pellet, cm^{-1}): 1676 (vs), 1614 (m), 1572 (vs), 1535 (vs), 1495 (vs), 1466 (m), 1394 (vs), 1344 (vs), 1275 (s), 1256 (vs), 1184 (m), 1140 (m), 1005 (m), 930 (m), 905 (m), 881 (m), 856 (s), 806 (s), 791 (s), 766 (m), 735 (s), 712 (s), 623 (s), 548 (s), 496 (s), 442 (s).

[Nd(HBtec)]$_n$ (*Nd-conv*). Yield: 0.260 g (55 **%**). Anal. Calcd for $NdC_{10}O_8H_2$ (%): C, 30.4; H, 0.50. Found: C, 30.5; H, 0.52. IR (KBr pellet, cm^{-1}): 1676 (vs), 1612 (m), 1570 (vs), 1529 (vs), 1493 (vs), 1454 (m), 1389 (vs), 1339 (vs), 1269 (s), 1258 (vs), 1180 (m), 1138 (m), 1001 (m), 932 (m), 905 (m), 876 (m), 851 (s), 806 (s), 793 (s), 766 (m), 729 (s), 712 (s), 621 (s), 546 (s), 496 (s), 432 (s).

[Sm(HBtec)]$_n$ (*Sm-conv*). Yield: 0.260 g (41 **%**). Anal. Calcd for $SmC_{10}O_8H_2$ (%): C, 30.0; H, 0.50. Found: C, 29.7; H, 0.31. IR (KBr pellet, cm^{-1}): 1676 (vs), 1612 (m), 1570 (vs), 1531 (vs), 1493 (vs), 1458 (m), 1391 (vs), 1340 (vs), 1271 (s), 1256 (vs), 1182 (m), 1140 (m), 1001 (m), 932 (m), 905 (m), 878 (m), 853 (s), 806 (s), 793 (s), 766 (m), 731 (s), 712 (s), 621 (s), 546 (s), 496 (s), 436 (s).

[Y(HBtec)]$_n$ (*Y-conv*). Yield: 0.142 g (56 **%**). Anal. Calcd for $YC_{10}O_8H_2$ (%): C, 35.4; H, 0.59. Found: C, 34.9; H, 0.44. IR (KBr pellet, cm^{-1}): 1678 (vs), 1614 (m), 1574 (vs), 1535 (vs), 1495 (vs), 1468 (m), 1394 (vs), 1346 (vs), 1277 (s), 1254 (vs), 1184 (m), 1140 (m), 1005 (m), 932 (m), 905 (m), 883 (m), 858 (s), 808 (s), 791 (s), 766 (m), 735 (s), 712 (s), 623 (s), 548 (s), 498 (s), 446 (s).

[Er(HBtec)]$_n$ (*Er-conv*). Yield: 0.187 g (60 %). Anal. Calcd for $ErC_{10}O_8H_2$ (%): C, 28.8; H, 0.48. Found: C, 28.1; H, 0.26. IR (KBr pellet, cm^{-1}): 1676 (vs), 1614 (m), 1574 (vs), 1535 (vs), 1495 (vs), 1468 (m), 1394 (vs), 1346 (vs), 1281 (s), 1254 (vs), 1184 (m), 1140 (m), 1007 (m), 930 (m), 903 (m), 883 (m), 858 (s), 806 (s), 791 (s), 766 (m), 735 (s), 712 (s), 623 (s), 548 (s), 496 (s), 444 (s).

[Ce(HBtec)]$_n$ (*Ce-conv*). Yield: 0.187 g (46 %). Anal. Calcd for $CeC_{10}O_8H_2$ (%): C, 30.8; H, 0.52. Found: C, 30.7; H, 0.61. IR (KBr pellet, cm^{-1}): 1676 (vs), 1612 (m), 1570 (vs), 1529 (vs), 1493 (vs), 1450 (m), 1389 (vs), 1337 (vs), 1258 (vs), 1180 (m), 1138 (m), 999 (m), 934 (m), 907 (m), 872 (m), 849 (s), 806 (s), 793 (s), 766 (m), 727 (s), 712 (s), 619 (s), 546 (s), 496 (s), 428 (s).

Synthesis of microcrystalline powder. Microwave heating was performed on CEM discover SP system.

A mixture of $Ln(NO_3)_3 \cdot xH_2O$ (0.75 mmol), 1,2,4,5-benzenetetracarboxylic acid (381.2 mg, 1.5 mmol) and H_2O (15 mL) was placed in a 35 mL borosilicate reactor. Then, the mixture was heated in microwave oven at 180° C for 30 min for Ln = Eu, at 190°C for 30 min for Ln = Dy and Sm, and for 190°C/1h for Er and Y. The microwave power was fixed at 200 W. A powder was finally recovered by filtration and washed successively with H_2O and EtOH.

[Eu(HBtec)]$_n$ (*Eu-MW*). Yield: 0.185 g (**42%**). Anal. Calcd for $EuC_{10}O_8H_2$ (%): C, 29.9; H, 0.50. Found: C, 29.3; H, 0.66.

[Dy(HBtec)]$_n$ (*Dy-MW*). Yield: 0.175 g (**41%**). Anal. Calcd for $DyC_{10}O_8H_2$ (%): C, 29.1; H, 0.49. Found: C, 28.3; H, 0.56.

[Sm(HBtec)]$_n$ (*Sm-MW*). Yield: 0.187 g (**42%**). Anal. Calcd for $SmC_{10}O_8H_2$ (%): C, 30.0; H, 0.50. Found: C, 29.4; H, 0.43.

[Er(HBtec)]$_n$ (*Er-MW*). Yield: 0.200 g (**45 %**). Anal. Calcd for $ErC_{10}O_8H_2$ (%): C, 28.8; H, 0.48. Found: C, 28.1; H, 0.43.

[Y(HBtec)]$_n$ (*Y-MW*). Yield: 0.034 g (**8 %**). All attempts for a better yield have failed. Anal. Calcd for $YC_{10}O_8H_2$ (%): C, 35.4; H, 0.59. Found: C, 34.3; H, 0.55.

Characterization. Powder X-ray Diffraction spectra were monitored using a D8 Bruker diffractometer in the Bragg-Brentano geometry, equipped with a front germanium monochromator, a copper anode (Cu*K*-L3 radiation λ=1.540598 Å) and a LynxEye PSD detector. Thermogravimetric analysis (TGA) were performed by flowing dry air with a heating and cooling rate of 5°C/min on a SETARAM TG-DSC 111 from 25 to 800°C. Fourier transform infrared (FT-IR) spectra were recorded in the 4000-400 cm^{-1} range on a Bruker Vertex FTIR spectrometer equipped with a computer control using the OPUS software. Elemental analyses of the solids were performed by the "Service Chromato-Masse Microanalyse" at BioCIS in Châtenay-Malabry (France). Photoluminescence spectra were recorded on a Jobin-Yvon Fluorolog 3 fluorometer equipped with a photomultiplier (excitation source: 450 W Xe arc lamp) using the front face acquisition mode. The emission spectra were corrected for detection and optical spectral response of the spectrofluorimeter and the excitation spectra were weighed for the spectral distribution of the lamp intensity using a photodiode reference detector. Photoluminescence Quantum Yield measurements were recorded at room temperature with a Horiba quanta-phi integrating sphere optically connected with the Fluorolog 3 through fibres. CIE parameters were calculated with the script CIEgui [30] developed on Matlab® software. The morphology of powder was investigated with a field-emission gun scanning electron microscope JEOL JSM7600F operating at 7 kV.

Single-crystal X-ray diffraction was performed with a Bruker Nonius X8 diffractometer equipped with a CCD bidimensional detector using Mo Kα monochromatized radiation (λ = 0.71073 Å). The unit cell determination and data integration were carried out using the Supergui software. The structures were solved by using Olex2 [31] software with the SHELXS structure solution program and refined by full-matric least-squares on F^2 with SHELXL-97 [32,33] using an anisotropic model for non-hydrogen atoms. All H atoms attached to carbon were introduced in idealized positions (d_{CH} = 0.96 Å). Table 1 provides a summary of the crystallographic data together with refinement details for the novel compounds.

Results and discussion

Structural characterization

Crystals suitable for single-crystal X-ray diffraction analysis were obtained for all compounds by conventional hydrothermal synthesis (***Ln-conv***). According to X-ray crystallography, the chemical composition are in agreement with the following formula $[M(Hbtec)]_n$ and the compounds are isostructural of $[Tb(Hbtec)]_n$ [28] and $[Gd(Hbtec)]_n$ [34] already reported. All these coordination polymers crystallize in *P*-1 space group with very similar unit cell parameters (Table 1). Therefore, as an example, the crystal structure of $[Eu(Hbtec)]_n$ is chosen to describe the coordination framework in the series. The $[Eu(Hbtec)]_n$ compound has a 3D framework containing 9-coordinated europium centers EuO_9 forming a distorted monocapped square anti-prism (Figure 1a). In the crystal structure, the pyromellitic acid ligand is monoprotonated as confirmed by the FTIR analyses (Figure S2), which reveal the presence of the absorption peak centered at 1680 cm^{-1} associated with the dangling C=O bond [35]. Six $HBtec^{3-}$ ligands share nine oxygen atoms to the Eu^{3+} center with Eu─O distances ranging from 2.35 to 2.59 Å. In the structure, there are three different coordination modes, namely two tridentate-bridging-chelating modes, one bridging and one monodentate-chelating (Figure 1b). Each EuO_9 polyhedron are linked *via* edge-sharing along the *b* axis, forming 1D chains with a nearest Eu─Eu distance of 4.1397(9) Å (Figures 1c and 1d). To complete the final 3D framework, the $HBtec^{3-}$ ligands connect to four neighboring Eu^{3+} centers to form chains (Figure 1d). Furthermore, distances between the non-coordinated oxygen atom from the carboxylate ligand and the coordinated oxygen O_8 is equal to 2.8598 Å, indicating the presence of an hydrogen bond (Figure 1d) [36].

The chemical composition was confirmed by elemental and thermal analyses (Figure S3). The powder X-ray diffraction patterns of the whole series confirm that the experimental patterns perfectly match the simulated powder diffractograms calculated from the single crystal X-ray diffraction data (Figure S1) and that all compounds are isostructural.

Thermal and water stability

The thermogravimetric analyses (TGA) show that the $[Ln(Hbtec)]_n$ compounds have high thermal stability (Figure S3) with no weight loss observed before 400 °C for the whole series. Then, a mass loss of approximately 56 %, corresponding to the decomposition of the ligand and the formation of the corresponding lanthanide oxide Ln_2O_3, is observed around 500-550 °C for each compound except for Y counterpart that observes a mass loss of 67 % due to the different mass weight of the yttrium. The TGA curves also confirm the absence of coordinated or uncoordinated water molecules usually obtained in coordination polymers or MOFs compounds synthesized by hydrothermal procedures. Additionally, the $[Ln(Hbtec)]_n$ compounds exhibit a good water stability and can maintain their structure in water at least for one week, which can be confirmed by the powder X-ray diffraction analyses (Figure S4). Finally, the water stability was also investigated for various pH ranging from 4 to 11. After immersing in the different aqueous solution during 1 day, any structural modification was observed on the XRD patterns (Figure S5).

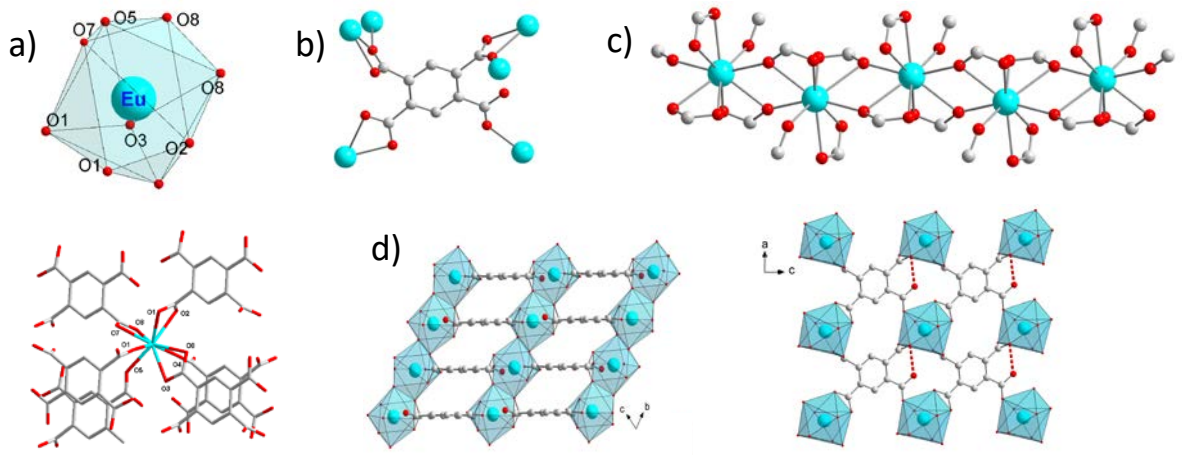

Figure 1. a) (top) coordination sphere of Eu in $[Eu(Hbtec)]_n$ forming a distorted tricapped trigonal prism and (down) representation of the asymmetric unit, b) Coordination mode of the pyromellitic carboxylate, c) Representation of chains formed by edge-connected EuO_9 polyhedra, d) Projections along the *a* axis and the *b* axis of the$[Eu(Hbtec)]_n$ structure (light blue: EuO_9 polyhedra, red: oxygen, grey: carbon, H atoms being omitted for clarity). H-bond between the non-coordinated oxygen atom of the linker and one coordinated oxygen (O_8) is represented in dotted red line.

Table 1. Crystal data and structure refinement for the $[Ln(Hbtec)]_n$ compounds.

	Eu	***Sm***	***Dy***	***Nd***	***Er***	***Ce***	***Y***
Empirical Formula	$EuC_{10}H_3O_8$	$SmC_{10}H_3O_8$	$DyC_{10}H_3O_8$	$NdC_{10}H_3O_8$	$ErC_{10}H_3O_8$	$CeC_{10}H_3O_8$	$YC_{10}H_3O_8$
Formula weight	402.08	400.47	411.10	394.36	417.38	390.24	321.01
Crystal system	Triclinic	Triclinic	Triclinic	Triclinic	Triclinic	Triclinic	Triclinic
Space group	P-1	P-1	P-1	P-1	P-1	P-1	P-1
a/Å	7.2196(14)	7.2510(15)	7.1888(14)	7.2905(15)	7.1615(14)	7.3690(15)	7.1891(2)
b/ Å	7.9894(16)	8.0409(16)	7.9260(16)	8.1100(16)	7.8797(16)	8.2100(16)	7.9155(2)
c/ Å	8.7448(17)	8.7870(18)	8.7753(18)	8.7722(18)	8.7575(18)	8.7580(18)	8.7796(2)
α/°	65.66(3)	65.34(3)	65.42(3)	65.35(3)	65.37(3)	65.25(3)	65.421(3)
β/°	86.22(3)	86.28(3)	86.35(3)	86.10(3)	86.38(3)	86.03(3)	86.384(2)
γ/°	84.32(3)	84.33(3)	84.45(3)	84.26(3)	84.49(3)	84.03(3)	84.406(2)
Volume/ $Å^3$	457.13(19)	463.16(19)	452.43(19)	468.8(2)	447.08(19)	478.4(2)	452.03(2)
Z	2	2	2	2	2	2	2
ρcalc (g/cm^3)	2.921	2.872	3.018	2.794	3.101	2.709	2.358
Reflections collected	18331	10596	16283	10824	4107	6147	11993
Unique reflections	3968	3990	3931	4068	3279	3455	2395
(R_{int})	(0.0957)	(0.0611)	(0.0471)	(0.1172)	(0.0428)	(0.0993)	(0.0447)
GooF on F^2	0.986	1.078	1.067	1.016	0.744	0.988	1.073
R_1 (R_{int})	0.0340	0.0442	0.0336	0.0619	0.0738	0.0859	0.0338
wR_2 (I>=2σ (I))	0.0483	0.0802	0.0565	0.1015	0.1839	0.2045	0.0835
R_1 (all data),	0.0672	0.0737	0.0510	0.1229	0.1417	0.1855	0.0405
wR_2 (all data)	0.0538	0.0883	0.0607	0.1219	0.2523	0.3078	0.0859
CCDC number	**2058602**	**2058598**	**2058597**	**2058601**	**2058600**	**2058596**	**2058599**

Synthesis with microwave-assisted heating

Microcrystalline powders have been obtained by using hydrothermal route with microwave-assisted heating for Ln = Eu, Dy, Sm, Y, and Er (***Ln-MW***). Despite many attempts, Nd and Ce counterparts have been never obtained as pure phase in these conditions. Contrary to the conventional heating in an oven, microwave heating enables to considerably reduce the synthesis time (30 min-1h) due to a more homogeneous heating in the vessel while maintaining similar chemical yields (See experimental section). The phase purity was confirmed by X-ray diffraction (Figure S6), FTIR (Figure S7) and thermal analyses (Figure S8). The morphology was assessed by SEM analyses to identify the effect of the time synthesis reduction on the grain size. Therefore, SEM analyses evidence the formation of micronic powders with inhomogeneous morphology (Figure 2 and Figure S9), most of grains consisting in relatively thick platelet.

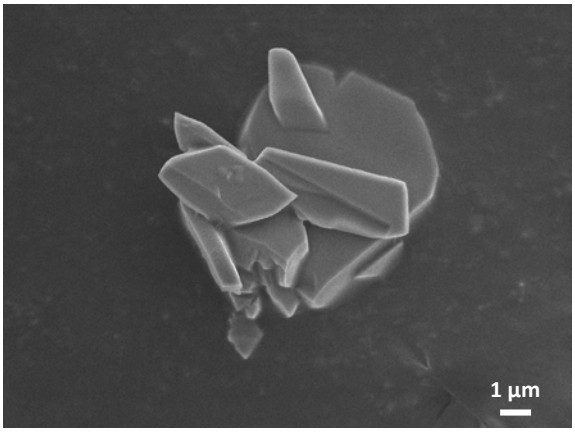

Figure 2. SEM image of the ***Eu-MW*** compound.

To go further, attempts were performed to reduce the grain size of powders by varying different synthetic parameters. As a proof-of-concept, this investigation has been only carried out on $[Eu(Hbtec)]_n$. Herein, we investigated the effect of four parameters: a) synthesis temperature and duration, b) europium precursor nature, c) microwave power, and d) addition of a steric agent. Synthesis temperature and duration were firstly tuned but a diminution of the temperature to 170°C or a reduction of the duration to 15 minutes lead in both cases to the formation of a secondary phase $[Eu_2(Btec)(H_2Btec)(H_2O)_2]_n$ (Figure S10), which is already reported in the literature with other lanthanide counterparts[27,34,37–40]. Thus, the synthesis temperature and duration were fixed at 180°C and 30 minutes, respectively, during the investigation of the three others parameters.

Attempts were performed with different europium precursors, which were chosen according their various solubility in water. Indeed, the influence of precursors was highlighted for numerous nanomaterials such as perovskites, metal oxides and semiconductor quantum dots, showing precursor-dependent growth kinetics under microwave conditions.[41] Thus, europium nitrate, chloride, acetate, trifluoroacetate and oxide were used under previously optimized reaction conditions. XRD analyses (Figure S11) evidence that the use of highly soluble lanthanide salts (nitrate or chloride) lead to the formation of the expected compound $[Eu(Hbtec)]_n$ while less soluble or insoluble precursors (acetate and oxide, respectively) cause the formation of another coordination polymer, namely $[Eu_2(Btec)_{1.5}(H_2O)]_n$ [22]. Furthermore, trifluoroacetate precursor leads to the formation of a mixed-phase corresponding to $[Eu_2(Btec)_{1.5}(H_2O)]_n$ (only some peaks are observed), as for the acetate and oxide precursors, and a secondary phase corresponding to $[Eu_2(Btec)(H_2Btec)(H_2O)_2]_n$ previously observed for a synthesis temperature of 170 °C or a duration of 15 min.

The effect of the microwave power was also tested for 25, 50, 100 and 200 W. During microwave-assisted syntheses, the power has an impact on the heating rate to reach the targeted temperature (180°C), and consequently in the growth kinetics. The duration to reach 180 °C is 50, 25, 5, and 3 min for 25, 50, 100, and 200 W respectively. XRD analyses confirm that the expected compound $[Eu(Hbtec)]_n$ is obtained for microwave powers ranging from

50 to 200 W (Figure 3). The diffraction patterns show a slight increase of the peaks width when the microwave power decreases, corresponding to the decrease of the MOFs crystallites size and overall crystallinity (Figure S12). Nevertheless, any morphological change can be observed on SEM images (Figure S13). Finally, at very low power (25W), the synthesis leads to the formation of another phase with chain topology $\{[Eu_2(H_2btec)(btec)(H_2O)].4H_2O\}_n$ already reported in the literature.[42]

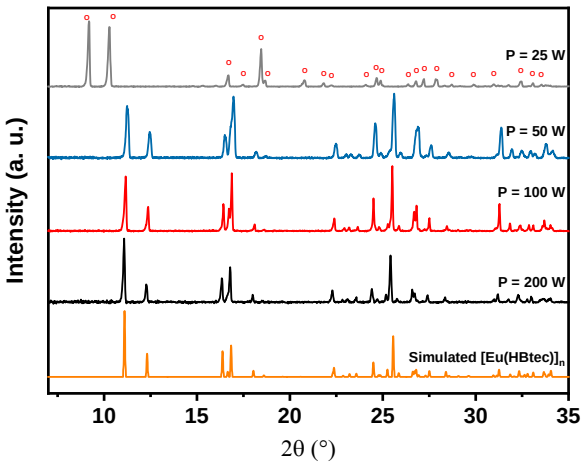

Figure 3. X-ray diffraction pattern of ***Eu-MW*** obtained by microwave-assisted synthesis for different microwave powers (t = 30 min, T = 180 °C, $Eu(NO_3)_3$, x H_2O).

Finally, the effect of the addition of different ionic and nonionic steric agents (1 equivalent compared to the metal concentration) that are soluble or miscible with water was studied in the previous optimized synthesis conditions. Note that it is usually preferable to reduce concentration to perform such experiments in order to favor the nucleation instead of grain growth. However, in our case, a diminution of the metal concentration leads to the formation of others coordination polymers. Thus, the concentration was kept constant at 0.05 M. Here, the strategy consists in using ionic and non-ionic surfactants that have been already used by the MOF community to control the growth and shape of MOFs powders[43–46], such as polyvinylpyrrolidone (PVP) and polyethylene glycol (PEG). Thus, four different surfactants have been used, namely polyethylene glycol (PEG) with different average molar weight (200, 400 and 1000 $g.mol^{-1}$), hexadecyltrimethylammonium bromide (CTAB), octylphenoxy poly(ethyleneoxy)ethanol (IGEPAL CA-630) and polyvinylpyrrolidone (PVP10, average molar weight of 10 000 $g.mol^{-1}$) (Figure S14)**.** First, XRD analyses (Figure S15) reveal that the use of PEG 200 leads to the expected compound $[Eu(Hbtec)]_n$ with no significant change in the XRD pattern compared to the reference compound, and thus no size decrease. The use of PEG 400 and PEG 1000 both lead to a mixed-phase including the expected one and a secondary phase corresponding to $[Eu_2(Btec)(H_2Btec)(H_2O)_2]_n$ better observed for the synthesis with PEG 1000. Then, the use of CTAB leads to a mixed-phase, similar to the ones observed for the syntheses with PEG 400 or 1000, that corresponds to a mixture between the expected compound $[Eu(Hbtec)]_n$ and some impurities of two other phases, namely the compounds $[Eu_2(Btec)_{1.5}(H_2O)]_n$ and $[Eu_2(Btec)(H_2Btec)(H_2O)_2]_n$. Finally, the use of PVP and IGEPAL CA-630, which have similar structure, lead both to the formation of $[Eu_2(Btec)(H_2Btec)(H_2O)_2]_n$ with dimer topology and two different secondary phases (Figure S15).

To conclude, the use of surfactants reveals that four phases are in competition, which is due to the versatility of the ligand that possesses four carboxylic groups allowing various coordination modes.[41,43,44] Thus, the addition of steric agents has an impact on the coordination process with the formation of coordination polymers getting less coordinated inorganic network (notably dimers) than chains. Therefore, the size reduction of $[M(Hbtec)]_n$ compounds by using classical surfactants seems to be not trivial.

Luminescence properties

Solid-state luminescence properties have been investigated for the ***Eu-conv***, ***Dy-conv*** and ***Sm-conv*** compounds at room-temperature. First, the phosphorescence spectrum at 77 K (Figure S16) of $[Y(Hbtec)]_n$ was recorded to identify the lowest-lying triplet energy state positioning of the organic ligand, which is estimated to be 25380 cm^{-1} from the shortest-wavelength .Thus, the pyromellitic ligand exhibit a T_1 level which is in a suitable energy range to sensitize Eu^{3+}, Dy^{3+}, and Sm^{3+}. Moreover, this value is in a perfect agreement with the one already reported in the literature.[29] All emission spectra of the three compounds were recorded upon excitation at 309 nm (Figure 4), and they contain the typical f-f sharp lines of considered Ln^{3+} ion (Figure S17). Then, the ***Sm-conv*** emission spectrum exhibits four characteristic transitions which correspond to the $^4G_{5/2} \rightarrow {}^6H_J$ transitions (with J = 5/2, 7/2, 9/2 and 11/2) leading to an orange emission (Figure S18) with CIE parameters equal to (0.606; 0.392). For the ***Dy-conv*** , emission spectrum is composed by the three transitions $^4F_{9/2} \rightarrow {}^6H_J$ (with J = 15/2, 13/2 and 11/2), which leads to a yellow emission . The main transition responsible for its yellow emission color (Figure S18) with CIE parameters equal to (0.387; 0.426). For both compounds, the emission is not visible with naked eye due to their weak emissions, short lifetimes and thus poor observed quantum yields (< 1 %). This can be explained by the small energy gaps between the emitting state of the lanthanide ion and the highest sub-level of its ground state, or receiving, multiplet.[47] The smaller this gap is, the easier non-radiative deactivations can occur. Thus, these energy gaps of 7200 cm^{-1} for Sm^{3+} ($^4G_{5/2} \rightarrow {}^6F_{11/2}$) and 7500 cm^{-1} for Dy^{3+} ($^4F_{9/2} \rightarrow {}^6F_{3/2}$) are too short to generate efficient emission transition compared to Eu^{3+} with a gap of 12000 cm^{-1} ($^5D_0 \rightarrow {}^7F_6$) (Figure S17). On the other hand, the ***Eu-conv*** compound exhibits an intense red emission with good lifetime (τ_{obs} = 1.390 ± 0.005 ms) that is due to the $^5D_0 \rightarrow {}^7F_2$ main transition. Emission spectrum is composed by four emission transitions that correspond to the $^5D_0 \rightarrow {}^7F_J$ transitions (with J = 1, 2, 3 and 4)[48], which leads to a red emission (Figure S18) with CIE parameters equal to (0.656; 0.344). Moreover, it can be pointed out that the quantum yield of the ***Eu-conv*** compound is rather good (Φ_{obs} = 25 %) compared to those found in the literature for other coordination polymers.[49–51] This can be explained by the absence of coordinated or uncoordinated water molecules usually present in MOFs compounds synthesized by hydrothermal routes. Indeed, water molecules, and more particularly O-H vibrators promote non-radiative deactivation processes and thus luminescence quenching.

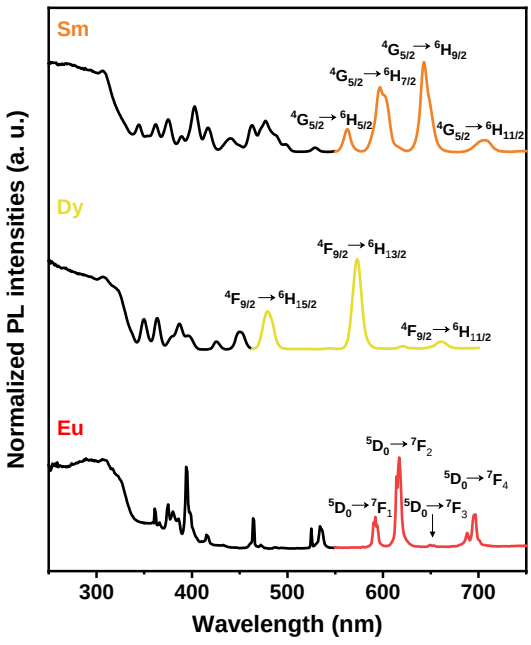

Figure 4. Excitation (black lines) and emission spectra (coloured lines) of $[M(HBtec)]_n$ with M = Sm, Dy and Eu.

Conclusion

A new series of coordination polymers have been successfully obtained with the 1,2,4,5-benzentetracarboxylic acid as ligand. With the chemical composition $[M(HBtec)]_n$, the compounds do not contain any coordinated and non-coordinated water molecules, and consequently they exhibit a huge thermal stability under air compared to others reported Ln-coordination polymers. Moreover, their high water stability in a wide pH range make them very promising for chemical sensing, especially the Eu compound which exhibits good quantum yield.

Appendix A. Supplementary data

CCDC 2058596-2058602 contains the supplementary crystallographic data for <yyy>. These data can be obtained free of charge via http://www.ccdc.cam.ac.uk/conts/retrieving.html, or from the Cambridge Crystallographic Data Centre, 12 Union Road, Cambridge CB2 1EZ, UK; fax: (+44) 1223-336-033; or e-mail: mailto:deposit@ccdc.cam.ac.uk.

Acknowledgements

This works was supported by the French National Research Agency (ANR) who financial supports the project ANR-18-CE09-0008-01.

Keywords: coordination polymers • lanthanide • water stability • thermal stability • luminescence

References

1 M. Eddaoudi, J. Kim, N. Rosi, D. Vodak, J. Wachter, M. O'Keeffe and O. M. Yaghi, *Science (80-.).*, 2002, **295**, 469–472.

2 Y.-B. Zhang, H. Furukawa, N. Ko, W. Nie, H. J. Park, S. Okajima, K. E. Cordova, H. Deng, J. Kim and O. M. Yaghi, *J. Am. Chem. Soc.*, 2015, **137**, 2641–2650.

3 T. M. Reineke, M. Eddaoudi, M. O'Keeffe and O. M. Yaghi, *Angew. Chemie - Int. Ed.*, 1999, **38**, 2590–2594.

4 T. Devic, V. Wagner, N. Guillou, A. Vimont, M. Haouas, M. Pascolini, C. Serre, J. Marrot, M. Daturi, F. Taulelle and G. Férey, *Microporous Mesoporous Mater.*, 2011, **140**, 25–33.

5 X. Zhang, Z. Chen, X. Liu, S. L. Hanna, X. Wang, R. Taheri-Ledari, A. Maleki, P. Li and O. K. Farha, *Chem. Soc. Rev.*, 2020, 49, 7406–7427.

6 N. S. Bobbitt, M. L. Mendonca, A. J. Howarth, T. Islamoglu, J. T. Hupp, O. K. Farha and R. Q. Snurr, *Chem. Soc. Rev.*, 2017, 46, 3357–3385.

7 J. Lee, O. K. Farha, J. Roberts, K. A. Scheidt, S. T. Nguyen and J. T. Hupp, *Chem. Soc. Rev.*, 2009, **38**, 1450–1459.

8 M. Kumar, L.-Q. Li, J. K. Zareba, L. Tashi, S. C. Sahoo, M. Nyk, S.-J. Liu and H. N. Sheikh, *Cryst. Growth Des.*, 2020, **20**, 6430–6452.

9 Y. Wu, Y. Zhou, S. Cao, P. Cen, Y.-Q. Zhang, J. Yang and X. Liu, *Inorg. Chem.*, 2020, **59**, 11930–11934.

10 W. Gao, A.-M. Zhou, H. Wei, C.-L. Wang, J.-P. Liu and X.-M. Zhang, *New J. Chem.*, 2020, **44**, 6747–6759.

11 J.-W. Zhang, S. Xu, S.-N. Liu, J. Hu, Y.-X. Qiao and B.-Q. Liu, *Eur. J. Inorg. Chem.*, 2020, **2020**, 1233–1241.

12 a Ben Khélifa, M. S. Belkhiria, G. Huang, S. Freslon, O. Guillou and K. Bernot, *Dalton Trans.*, 2015, **44**, 16458–64.

13 K. Binnemans, 2009, 4283–4374.

14 J. Rocha, C. D. S. Brites and L. D. Carlos, *Chem. – A Eur. J.*, 2016, **22**, 14782–14795.

15 C. D. S. Brites, P. P. Lima, N. J. O. Silva, A. Millán, V. S. Amaral, F. Palacio and L. D. Carlos, *New J. Chem.*, 2011, **35**, 1177.

16 X. Fan, S. Freslon, C. Daiguebonne, L. Le Pollès, G. Calvez, K. Bernot, X. Yi, G. Huang and O. Guillou, *Inorg. Chem.*, 2015, **54**, 5534–5546.

17 I. N'Dala-Louika, D. Ananias, C. Latouche, R. Dessapt, L. D. Carlos and H. Serier-Brault, *J. Mater. Chem. C*, 2017, **5**, 10933–10937.

18 C. Janiak, *J. Chem. Soc. Dalt. Trans.*, 2003, **3**, 2781–2804.

19 H.-C. Zhou and S. Kitagawa, *Chem. Soc. Rev.*, 2014, **43**, 5415–5418.

20 M. Eddaoudi, D. F. Sava, J. F. Eubank, K. Adil and V. Guillerm, *Chem. Soc. Rev.*, 2015, **44**, 228–249.

21 S. Freslon, Y. Luo, C. Daiguebonne, G. Calvez, K. Bernot and O. Guillou, *Inorg. Chem.*, 2016, **55**, 794–802.

22 M. G. Lahoud, R. C. G. Frem, L. F. Marques, G. Arroyos, P. Brandão, R. A. S. Ferreira and L. D. Carlos, *J. Solid State Chem.*, 2017, **253**, 176–183.

23 L. Canadillas-Delgado, J. Pasan, O. Fabelo, M. Julve, F. Lloret and C. Ruiz-Perez, *Polyhedron*, 2013, **52**, 321–332.

24 R. Cao, D. Sun, Y. Liang, M. Hong, K. Tatsumi and Q. Shi, *Inorg. Chem.*, 2002, **41**, 2087–2094.

25 C.-K. Xia, W. Sun, Y.-Y. Min, K. Yang and Y.-L. Wu, *Polyhedron*, 2018, **141**, 377–384.

26 Y. Luo, K. Bernot, G. Calvez, S. Freslon, C. Daiguebonne, O. Guillou, N. Kerbellec and T. Roisnel, *CrystEngComm*, 2013, **15**, 1882.

27 J.-J. Yang, X.-Y. Yu, Y.-H. Luo, H. Zhang and W.-P. Gao, *Inorg. Chem. Commun.*, 2015, **61**, 16–20.

28 M. A. Silva, N. R. de Campos, L. A. Ferreira, L. S. Flores, J. C. A. Júnior, G. L. dos Santos, C. C. Corrêa, T. C. dos Santos, C. M. Ronconi, M. V. Colaço, T. R. G. Simões, L. F. Marques and M. V. Marinho, *Inorganica Chim. Acta*, 2019, **495**, 118967.

29 D. Sun, R. Cao, Y. Liang, Q. Shi and M. Hong, *J. Chem. Soc. Dalt. Trans.*, 2002, 1847–1851.

30 P. Patil, 2021.

31 O. V. Dolomanov, L. J. Bourhis, R. J. Gildea, J. A. K. Howard and H. Puschmann, *J. Appl. Crystallogr.*, 2009, **42**, 339–341.

32 M. Sheldrick, G., Göttingen University, 1986.

33 M. Sheldrick, G., Göttingen University, 1997.

34 D. Sun, R. Cao, Y. Liang, Q. Shi and M. Hong, *J. Chem. Soc. Dalt. Trans.*, 2002, 1847–1851.

35 C. C. R. Sutton, G. da Silva and G. V. Franks, *Chem. - A Eur. J.*, 2015, **21**, 6801–6805.

36 Q.-D. Liu, J.-R. Li, S. Gao, B.-Q. Ma, F.-H. Liao, Q.-Z. Zhou and K.-B. Yu, *Inorg. Chem. Commun.*, 2001, **4**, 301–304.

37 S. Dao-Feng, B. Wen-Hua, C. Rong, L. Xing, S. Qian and H. Mao-Chun, *Chinese J. Chem.*, 2010, **21**, 405–408.

38 Y.-H. Wen, J. Zhang, Z.-J. Li, Y.-Y. Qin, Y. Kang, R.-F. Hu, J.-K. Cheng and Y.-G. Yao, *Acta Crystallogr. Sect. E Struct. Reports Online*, 2004, **60**, m535–m537.

39 L. Guo, G. Wu and H. H. Li, *J. Chem. Crystallogr.*, 2012, **42**, 192–198.

40 C. Y. Li, D. M. Cai, J. C. Yin, L. P. Cai, M. Zeng, J. Wang and W. H. Zhu, *Russ. J. Coord. Chem. Khimiya*, 2016, **42**, 476–485.

41 I. Halimi, E. M. Rodrigues, S. L. Maurizio, H. Q. T. Sun, M. Grewal, E. M. Boase, N. Liu, R. Marin and E. Hemmer, *J. Mater. Chem. C*, 2019, **7**, 15364–15374.

42 C. De Wu, C. Z. Lu, W. Bin Yang, S. F. Lu, H. H. Zhuang and J. S. Huang, *Eur. J. Inorg. Chem.*, 2002, **2**, 797–800.

43 C. Huang, H. Wang, X. Wang, K. Gao, J. Wu, H. Hou and Y. Fan, *Chem. - A Eur. J.*, 2016, **22**, 6389–6396.

44 B. Zhou, L. M. Liang and J. Yao, *J. Solid State Chem.*, 2015, **223**, 152–155.

45 H. P. Nguyen Thi, H. D. Ninh, C. Van Tran, B. T. Le, S. V. Bhosale and D. D. La, *ChemistrySelect*, 2019, **4**, 2333–2338.

46 J. Gao, K. Ye, M. He, W. W. Xiong, W. Cao, Z. Y. Lee, Y. Wang, T. Wu, F. Huo, X. Liu and Q. Zhang, *J. Solid State Chem.*, 2013, **206**, 27–31.

47 S. V. Eliseeva and J.-C. G. Bünzli, *Chem. Soc. Rev.*, 2010, **39**, 189–227.

48 K. Binnemans, *Coord. Chem. Rev.*, 2015, **295**, 1–45.

49 Y. Lu and B. Yan, *Chem. Commun.*, 2014, **50**, 13323–13326.

50 D. T. de Lill, A. de Bettencourt-Dias and C. L. Cahill, , DOI:10.1021/IC062019U.

51 P. Yi, H. Huang, Y. Peng, D. Liu and C. Zhong, *RSC Adv.*, 2016, **6**, 111934–111941.